Annadate *et al.*
*Environmental Sciences Europe* (2025) 37:40
https://doi.org/10.1186/s12302-025-01081-1

Environmental Sciences Europe

RESEARCH

Open Access

# Monitoring the impact of EU F-gas regulation on HFC-134a emissions through a comparison of top-down and bottom-up estimates

Saurabh Annadate[1,2,3*], Enrico Mancinelli[1], Barbara Gonella[4], Federica Moricci[4], Simon O'Doherty[5], Kieran Stanley[5], Dickon Young[5], Martin K. Vollmer[6], Rita Cesari[7], Serena Falasca[8], Umberto Giostra[1], Michela Maione[1,3] and Jgor Arduini[1,3*]

## Abstract

HFC-134a is the most prevalent hydrofluorocarbon used as a replacement for ozone-depleting CFCs and HCFCs. Due to its high global warming potential, it is regulated under various European and global frameworks, underscoring the importance of tracking its emissions. Emissions derived by the commonly used, bottom-up, methodology are affected by a certain degree of uncertainty. The bottom-up estimates can be aided with an independent top-down estimate based on atmospheric observations combined with an atmospheric transport model. This study presents HFC-134a emissions for Europe, with a specific focus on Italy, from 2008 to 2023. The emissions were estimated using a Bayesian inversion methodology, based on atmospheric observations collected at four European stations. Our analysis reveals a slightly increasing trend in HFC-134a emissions for Italy from 2008 to 2015 of 0.17 Gg $yr^{-1}$, followed by a steady decrease thereafter, highlighting the effect of European regulation on fluorinated gases that came into force in 2014. We observed a reduction in HFC-134a emissions in the Po Basin inferred from the inversion method for 2020, likely due to mobility restrictions imposed during the COVID-19 pandemic. The observed mild seasonality in emissions may be partly attributed to higher air-conditioning activity during summer. Comparison with the Italian National Emission Inventory indicates an improvement in iterative bottom-up estimates, with the 2024 inventory emission trend post-2015 aligning closely with our inversion results. This study emphasises the need for collaboration between the two independent approaches to enhance the accuracy of emission estimates. Such cooperation is crucial to narrowing the gap in quantifying emissions of potent greenhouse gases and effectively assessing the progress of international policies and regulations.

**Keywords** Greenhouse gas emissions, Inverse modelling, Bottom-up inventories, EU F-gas regulation

*Correspondence:
Saurabh Annadate
saurabh.annadate@iusspavia.it
Jgor Arduini
jgor.arduini@uniurb.it
Full list of author information is available at the end of the article

## Introduction

Hydrofluorocarbons (HFCs) are a class of greenhouse gases (GHGs) primarily used as substitutes for ozone-depleting substances (ODSs) like chlorofluorocarbons (CFCs) and hydrochlorofluorocarbons (HCFCs). While HFCs do not harm the ozone layer, they contribute to global warming due to their high global warming potential (GWP) [14]. In response to the urgency of addressing climate change and reducing the impact of GHGs, the United Nations Framework Convention on Climate Change (UNFCCC) set strict principles and commitments related to GHG emission reduction targets. These targets, essential for achieving the goal of limiting global temperature rise, are expressed as a percentage reduction from a baseline year. In addition, under the Kigali amendment to the Montreal Protocol on Substances that Deplete the Ozone Layer [35], more than 140 countries commit to cutting HFC production and consumption by more than 80% over the next 30 years, with developed countries (including Italy) targeting an 85% reduction by 2036. Transparency is a fundamental principle under the UNFCCC, ensuring openness and accountability in the actions taken by countries to address climate change. This principle requires participating nations to regularly report on their GHG emissions, mitigation measures, and progress toward their stated reduction targets. This is done by compiling National Emission Inventories (NEIs), which countries submit annually to the UNFCCC. NEI methodology is based on activity level data and emission factors (EFs), following the IPCC (Intergovernmental Panel on Climate Change) Guidelines [15]. This methodology is affected by a certain degree of uncertainty that, according to the IPCC Guidelines, can be reduced thanks to a comparison with top-down estimates based on atmospheric observations combined with atmospheric transport model (inverse modelling) [18], especially if a sufficiently dense observation network is available. These models' accuracy and spatial resolution have improved over time, allowing for estimates of fluxes down to the country scale. For this reason, an increasing number of countries are including top-down estimates in their NEIs, which help identify possible uncertainties in EFs and ensure more accurate and transparent emission estimates [31].

This study focuses on 1,1,1,2-tetrafluoroethane ($CF_3CH_2F$), also known as HFC-134a. It is the most abundant HFC in the global atmosphere, and its thermodynamic properties, similar to those of dichlorodifluoromethane (CFC-12), make it an efficient option in refrigeration and mobile air conditioning (MAC) systems. With a global abundance of 113 parts per trillion (dry air mole fraction in pmol/mol or ppt) in 2020 and a 100-year Global Warming Potential (GWP) of 1526, its radiative forcing in 2020 was $19.5 \pm 0.3$ mW m$^{-2}$, which makes HFC-134a the major contributor to the total HFC radiative forcing (44%) [13, 37]. According to [10], based on a simple box model global emissions of HFC-134a increased from 113 to 236 Gg yr$^{-1}$ between 2004 and 2018. As estimated from inverse analysis based on atmospheric measurements from the Advanced Global Atmospheric Gases Experiment (AGAGE) and National Oceanic and Atmospheric Administration (NOAA) global networks, the global HFC-134a emissions were $245 \pm 27$ Gg yr$^{-1}$ in 2020 [37]. The emission trend analysis showed that, after more than 20 years of near linear rise, the HFC-134a emission growth rate slowed between 2016 and 2020 [37], showing the efficiency of mitigation policies implemented in the last decade.

In the past years, regional inverse modelling studies reporting HFC-134a emissions from developed countries (Annex I parties of UNFCCC) have shown some differences between bottom-up and top-down estimates [4, 9, 12, 23, 24, 30, 32]. [31] suggested a revision of EFs from both MAC and non-refrigeration and air-conditioning systems in the UK based on a comparison between the estimates of HFC-134a emissions from the national inventory and the emissions evaluated through inverse modelling. These authors pointed out that the UK inventory was far overestimating annual HFC-134a emissions compared to other EU countries' estimations because of overestimating the frequency of refilling refrigeration systems.

In this study, using a top-down approach, we estimated the emissions of HFC-134a from the European domain, focusing on Italy, between 2008 and 2023. In Italy, HFC-134a is the highest contributor to fluorinated gas emissions for mobile air-conditioning and refrigeration [25]. In the considered time range, stringent regulations and directives to control the use and emission of HFCs have been implemented by the European Union (EU) coherently with the emission reduction targets set by UNFCCC (see Supplement). Our analysis relies on continuous measurements of HFC-134a with hourly resolution conducted at four European monitoring sites that are part of the AGAGE network [28]. Emissions are estimated using a Bayesian inversion method, based on FLEXINVERT+ [34], described in detail in [3], which allows for the localisation and quantification of emissions from the European domain down to the national level. Our results are compared with those of Italian National Emission Inventories (NEIs) over the same period, and differences between the top-down and bottom-up emission estimates are analysed.

## Methods

### Atmospheric measurements

Inversion methods for estimating GHG emissions rely heavily on high-quality ambient measurements. Currently, there are only 16 continuous measurement stations worldwide in the AGAGE network monitoring HFC-134a, of which 6 are located in Europe, with 2 of those stations being relatively new. In this study, we used HFC-134a measurements from four measurement stations namely Monte Cimone (CMN; northern Apennines, Italy), Jungfraujoch (JFJ; Swiss Alps, Switzerland), Tacolneston (TAC; east coast, United Kingdom), and Mace Head (MHD; west coast, Republic of Ireland) within the AGAGE network [28]. More details on the measurement sites and the analytical techniques used can be found in the Supplement. To get good emissions estimates, it is necessary to include measurements from the so-called background measuring sites and sites affected by recent pollution events. The geographical configuration of the stations used allows for describing both substantial regional-scale pollution in the air that has travelled from the populated and industrial regions of Europe and clean westerly air that has travelled across the North Atlantic Ocean. Figure 1 shows the locations of the measurement sites used in the inversion setup. For the inversions, these observations were averaged to 3-hourly values. We removed very high observation values to eliminate the influence of very local emissions and boundary layer dynamics, particularly for the mountain stations where highly polluted air is sampled during summer afternoons (see Supplement for details).

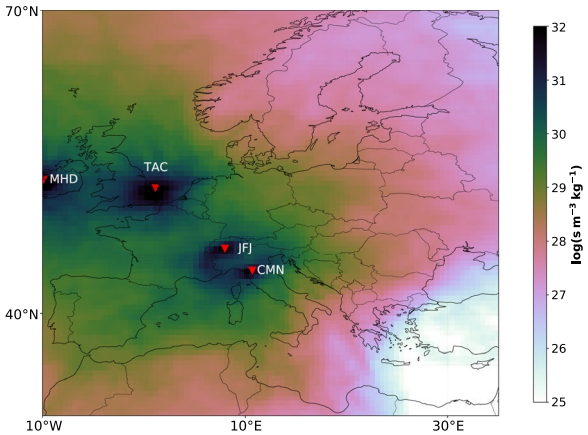


**Fig. 1** Total emission sensitivity calculated using the FLEXPART model for the year 2022 (red triangles indicate the receptor locations from where the particles were released)

### Bayesian inversion system

Atmospheric inversion uses high-frequency atmospheric measurements of the trace gases and a particle dispersion model to optimise the emission fluxes. The crucial element in this process is the relationship between the emissions and observations made at the receptor. It is also known as the source–receptor relationship (SRR). In this study, we have used the FLEXPART v10.4 [27] atmospheric transport model. 10,000 virtual particles are released from the receptor sites for each measurement and tracked for 10 days backwards in time. Figure 1 shows the total footprint obtained by summing the SRRs at the four receptor sites calculated at 3-h intervals for 2022. The map shows good sensitivity coverage over the northwestern European domain. Within the European domain, these four stations provide sufficient coverage for F-gas inverse modelling [4, 9, 20]. However, there are ongoing plans to establish additional observation stations in Eastern and Southern Europe to enhance sensitivity for inverse modelling methods. The main goal of the inversion process is to obtain an optimised distribution of gridded emissions. This optimised distribution seeks to reconcile observed mixing ratios by minimising the disparity between observed and simulated values constrained by the uncertainty ranges of the prior state variables. Within the Bayesian framework, under the assumption of Gaussian uncertainty distribution, achieving this optimised state involves minimising the following cost function $\mathbf{J}(\mathbf{x})$:

$$\mathbf{J}(\mathbf{x}) = \frac{1}{2}(\mathbf{x}-\mathbf{x_b})^T\mathbf{B}^{-1}(\mathbf{x}-\mathbf{x_b}) + \frac{1}{2}(\mathbf{Hx}-\mathbf{y})^T\mathbf{R}^{-1}(\mathbf{Hx}-\mathbf{y}), \quad (1)$$

where $\mathbf{B}$ represents the emission error covariance matrix, $\mathbf{R}$ denotes the observation error covariance matrix, and $\mathbf{x_b}$ stands for the vector of prior emissions. A comprehensive explanation of the error covariance matrices and their structure can be found in [34]. In our base inversions, the prior error covariance matrix $\mathbf{B}$ is formulated by assuming that each grid cell contains 100% of the prior emission flux value. The errors in the prior emission flux are assumed to be spatially and temporally correlated, with a spatial correlation length of 250 km over land and 1000 km over the sea. The temporal correlation length is assumed to be 90 days. More details on the inversion system are in the supplementary material.

### A priori emission information

In this study, we utilised the EDGAR v8.0 (Emissions Database for Global Atmospheric Research) dataset as the *a priori* information for HFC-134a [5]. This dataset offers yearly assessments of fluorinated gas emissions

from 1970 to 2022. The emissions of F-gases in this dataset have been determined through diverse channels, primarily relying on country-based declarations whenever possible. In cases where such data are unavailable, activity data statistics have been derived from UNEP data, scientific literature, and expert judgement [19]. The available gridded emissions, at a resolution of 0.1° × 0.1°, were regridded to a resolution of 0.5° × 0.5° to match the model resolution used in the inversion process. As the EDGAR v8.0 dataset provides emission fluxes up to 2022, we employed the same prior emission flux of 2022 for the inversion conducted for 2023. In one of the sensitivity tests, we replaced emission fluxes over Italy with the emissions reported to the UNFCCC in 2024 (disaggregated based on population density). Utilising the same inversion setup as in a previous study [3], demonstrated a significant consistency of the posterior results regardless of the use of different prior emission fields.

**The baseline definition**

The transport model can only account for mixing ratio changes caused by emissions within the chosen backward trajectory period. Therefore, we need to add the influence of the emission contributions before this time, which is usually referred to as the background mixing ratio or concentration in atmospheric inverse modelling. In our base inversion, we use the Robust Extraction of Baseline Signal (REBS) method introduced by [29] which is a statistical method using a robust local regression model to identify background contribution to the observed mixing ratios. In recent years, it has been used in various studies to determine a baseline for atmospheric inversions of several GHG species [1, 3, 4, 11, 20, 30, 32]. Figure 2 shows the baseline produced using the REBS method for three measurement stations for the inversion period of 2008 to 2023. We also use

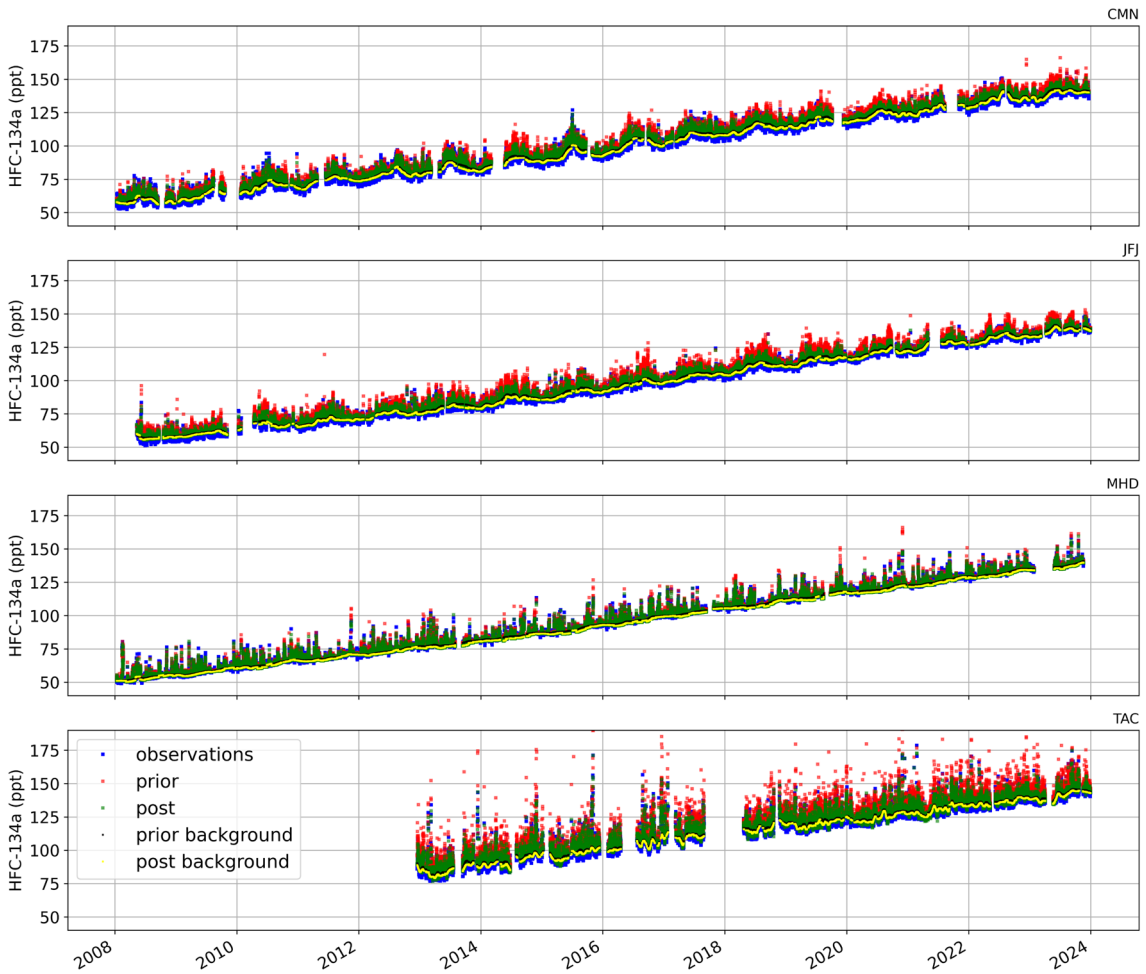


**Fig. 2** The modelled prior (in red) and posterior mixing ratios (in green) are compared against the observations (in blue) used in the inversion for the measurement sites of Monte Cimone (CMN), Jungfraujoch (JFJ), Mace Head (MHD), and Tacolneston (TAC) over the study period of 2008–2023. The background mixing ratios and the optimised background mixing ratios are in black and yellow, respectively

the "2-PDF" method [8] and Stohl's method [33] for baseline extraction for the sensitivity experiments.

### Sensitivity tests and inversions

In addition to the tests performed by [3], we conducted a series of sensitivity tests to finalise the inversion setup. We tested different temporal correlation scale lengths (30, 60, and 90 days) for the *a priori* uncertainties, various *a priori* uncertainties (70%, and 100%), different *a priori* fields (EDGAR v8.0 and UNFCCC), and different baseline extraction methods (REBS, 2-PDF method, and Stohl's method). The inversion setup proved stable across these tests, with the highest sensitivity observed in the use of different baseline methods. Consistent with [36], our tests showed that estimates based on Stohl's baseline were higher than those based on the REBS method. Estimates based on the 2-PDF and REBS baselines were very similar. To further evaluate the system's capability to predict seasonality and reduce inter-annual variability in emission estimates, we performed synthetic data experiments described in the supplementary material (Figures S3 and S4). Using the Bayesian inversion system and its components described above, we conducted yearly and monthly inversions covering the period from 2008 to 2023. Table S2 reports the number of observations used for inversions performed for each year.

## Results and discussion

### Inversion model performance

The comparisons between the prior and posterior modelled mixing ratios for the CMN, JFJ, MHD, and TAC measurement sites against the observations are depicted in Fig. 2. As seen in this figure, the variability in the prior mixing ratios compared to the observations is well captured by the FLEXPART transport model. Across all years, the Pearson correlation for the prior and the posterior modelled mixing ratios have improved significantly (Fig. 3). Table S2 reports the reduced $\chi^2$ index to assess the assumptions made about the uncertainties and error correlation scales used in **B** and **R** matrices for each inversion. The $\chi^2$ index is defined as the value of the cost function at the optimum [34]. The $\chi^2$ values for the inversions ranged from 0.86 to 1.25, where ideally it would be 1, indicating that the posterior solution is found within the prescribed uncertainties in **B** and **R** [34].

Figure 3 presents a Taylor diagram illustrating improvements in Pearson correlation and root mean squared (RMS) error for modelled mixing ratios across all ground measurement sites over all years. The length of the arrow in the Taylor diagram indicates the degree of improvements achieved by the inversion system in aligning the modelled mixing ratios with the observations. Significant improvements are observed in the CMN, JFJ, and TAC

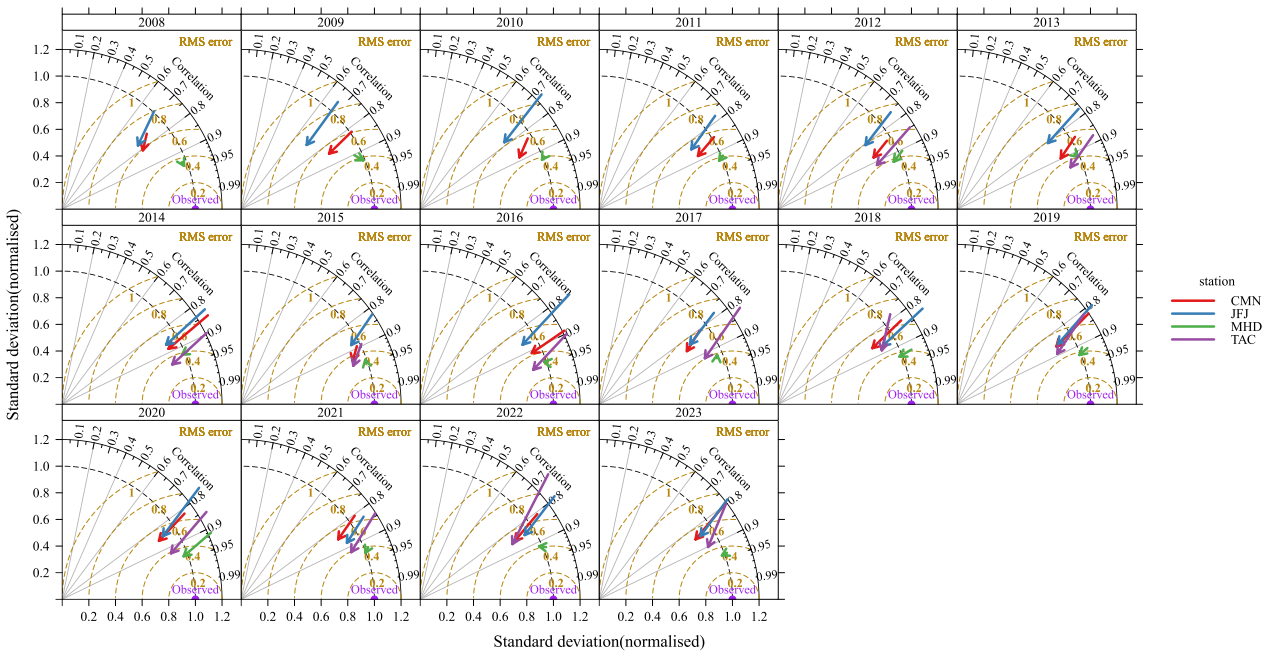


**Fig. 3** Taylor diagrams for comparing the prior and posterior simulated mixing ratios with observed mixing ratios for all the measurement stations and the years 2008–2023. Each arrow represents a station where the tail is prior and the head represents the posterior simulated mixing ratio. The radius along the *x*-axis and *y*-axis represents the normalised standard deviation against the mean mixing ratio. The azimuthal angle represents the Pearson correlation coefficient. The normalised (against observations) root mean square error (RMS) in the simulated mixing ratios is proportional to the distance from the point labelled "observed" (purple dot) on the *x*-axis which serves as a reference

modelled mixing ratios across all years. The Pearson correlation for the prior modelled mixing ratios ranged from 0.74 to 0.89 for CMN, 0.68 to 0.83 for JFJ, 0.9 to 0.95 for MHD, and 0.74 to 0.9 for TAC. Following inversion, the Pearson correlation for posterior modelled mixing ratios improved to 0.81–0.93 for CMN, 0.71–0.88 for JFJ, and 0.86–0.96 for TAC. MHD characterised as a background station, is best modelled by FLEXPART in contrast to the mountain sites. It showed the highest Pearson correlation values in the range of 0.91 to 0.95 and modest improvements after inversion.

### Optimised emission fluxes

Maps in Fig. 4, showing the prior and posterior emission fluxes for the 2022 inversion, highlight major emission hotspots over the modelling domain. The zoomed-over Italian domain in Fig. 4c shows the major Italian cities and the Po Valley, one of Europe's highest anthropised and industrialised areas, as the hot spots of HFC-134a emissions. Figure S5 shows disparities between the posterior and prior fluxes in the study domain and the relative reductions in error in the posterior estimates for 2022.

The spatial resolution and the emission sensitivity (Fig. 1) of the measurement network used in the inversions are better suited to analyse large emission sources rather than localised point sources. Therefore, we focused on a detailed analysis of the Po Valley region. Figure 5 specifically analyses the peculiarities of the year 2020. The average posterior emission flux for the period 2008–2019 (Fig. 5a) is compared with the posterior emission flux for 2020 (Fig. 5b). Figure 5c shows the emission anomaly for 2020, indicating a significant reduction in HFC-134a emissions over the Po Valley region. Generally, the Po Valley a posteriori emissions are adjusted to be higher than those reported in EDGAR v8.0 (data not shown). In 2020, Italy was severely affected by the COVID-19 pandemic, and stringent restrictions on citizens' mobility (lockdowns) were implemented, resulting in reduced emissions of a wide range of anthropogenic compounds. The Italian Environment Protection Agency (ISPRA, Istituto Superiore per la Protezione e Ricerca Ambientale) attributed the highest decrease in GHG emissions from the road transport sector to the reduction in passenger car traffic [17], with a reduction of 22% and 40% in total number of passengers and kilometres travelled, respectively, compared to the 2019 statistics [16]. In general, in 2020, over the Italian territory, the traffic volume was 27% lower compared to the million vehicle-kilometres travelled in 2019 [7]. Based on the average annual daily traffic dataset [2] for the road network managed by ANAS (Azienda Nazionale Autonoma delle Strade Statali), we estimated that in the Italian regions comprising the Po Valley (Piedmont, Lombardy, Veneto, and Emilia-Romagna) in 2020 the average annual daily traffic of light vehicles was 24% lower than 2019. [21] highlighted that use-phase emissions consist of three phases with different rates: regular fugitive emissions with a constant rate, irregular fugitive emissions, and emissions during MAC usage, which are higher than regular emissions. Operating MAC systems experience higher leakage rates due to increased pressure, thermal, and physical stress induced by the engine [39]. Additionally, the refrigerant mass flow rate varies with the speed of the compressor, which changes with driving conditions (e.g., idling, city driving, and high-speed mode). This suggests that the decrease in emissions in 2020 could be ascribed to a reduction in vehicle usage. This result demonstrates the usefulness of the

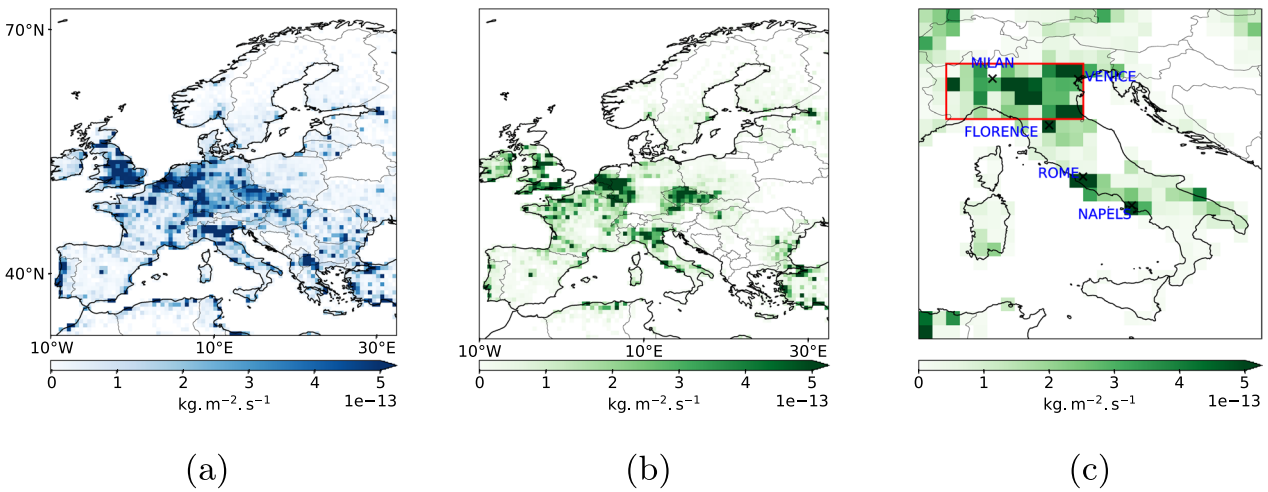


**Fig. 4** The a priori (**a**), and a posteriori (**b**) fluxes in the study domain, and a zoomed-in view of the a posteriori flux over Italy (**c**) for the year 2022. The Italian cities with emission hotspots are annotated and the Po Valley region is highlighted with a red box

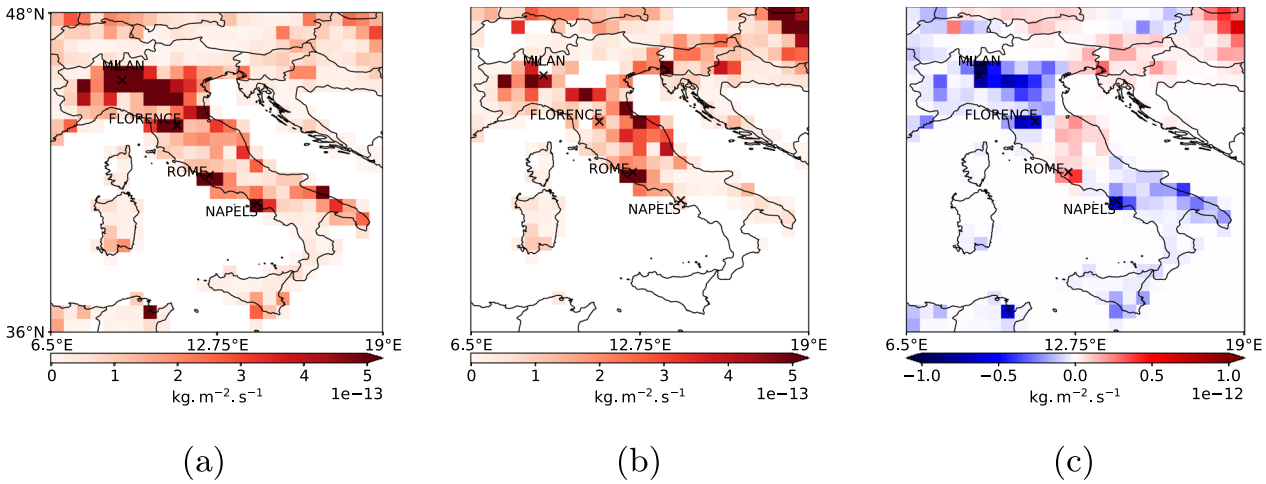


**Fig. 5** *a posteriori* emission flux over Italy (**a**) averaged between 2008 and 2019, (**b**) for the year 2020, which was affected by the COVID-19 pandemic, and (**c**) emission flux anomaly [**b**–**a**] between 2020 and 2008–2019

observation-based method in detecting emission changes that statistical methods cannot elucidate.

### Emission quantification

We aggregated the posterior emission fluxes to obtain yearly emissions. The final emission estimate and uncertainty incorporate results from five inversions. Alongside the base inversion, which employs the REBS baseline, EDGAR v8.0 prior, and 100% prior error uncertainty, we included two alternative baseline representations (2-PDF method and Stohl's method), one different prior emission field (UNFCCC), and one variation in prior error uncertainties (70%). The final estimate is the equally weighted mean of all the inversion estimates and the uncertainty is derived using Eq. (2):

$$\sigma = \sqrt{\frac{\sigma_1^2 + \sigma_2^2 + \cdots + \sigma_5^2}{5} + \sigma_s^2}, \tag{2}$$

where $\sigma_i$ (for $i = 1, 2, 3, 4, 5$) denotes the posterior uncertainty associated with each inversion and $\sigma_s$ denotes the standard deviation of the posterior uncertainty derived from all 5 inversions. Figure 6a illustrates the time series of inversion emission estimates for Italy, plotted along with the prior (EDGAR v8.0) emissions. Our results align with EDGAR v8.0 estimates up to 2015. Afterwards, our inversion-derived emissions show a decrease until 2020, followed by a rebound in 2021, whereas EDGAR estimates continue an increasing trend. The average emission of HFC-134a for the period 2008–2015 is 2.34 Gg $yr^{-1}$, with a yearly increasing trend of 0.17 Gg $yr^{-1}$. Subsequently, with a trend of −0.11 Gg $yr^{-1}$, the average emissions decreased by 26% to 1.73 Gg $yr^{-1}$ for the period 2016–2023. We estimate the highest emissions of HFC-134a in 2015 at $3.11 \pm 0.21$ Gg. According to the European Environment Agency report (2023) [6], concurrent with the adoption of F-Gas Regulation EU 517/2014, the total EU supply of HFC-134a increased by 55% in 2014 and by 18% in 2015, compared to 2013 (Figure S1). The sharp increase in the supply of HFC-134a in 2014 can be attributed to the EU market's response to the anticipated scarcity of HFC gases following the upcoming enforcement of the F-gas Regulation. This regulation introduced a quota system aimed at reducing the supply of HFCs across the EU beginning in 2015. In anticipation, the private sector engaged in extensive stockpiling efforts to secure HFCs before the regulation took effect. The lowest emissions were estimated for the last year of the study period, 2023, at $1.10 \pm 0.22$ Gg. These results suggest that the effectiveness of the F-Gas Regulation 517/2014, with the increased focus on refrigerant gas management, might have contributed to emission reductions. Technological improvements leading to lower leakage rates and better recovery practices might also have played a significant role.

Figure 6b presents a comparison between EDGAR v8.0 and the inversion estimates across the entire European domain. While there is a good agreement in the observed trends, the emission estimates from the inversion are consistently lower, with an average difference of 5.5 Gg $yr^{-1}$ compared to the EDGAR inventory. Table S3 reports our yearly inversion estimates for HFC-134a for the EU and Italy.

### Comparison between bottom-up and top-down Italian emission estimates

Compiling national inventories is a complex process requiring extensive information. Over the years,

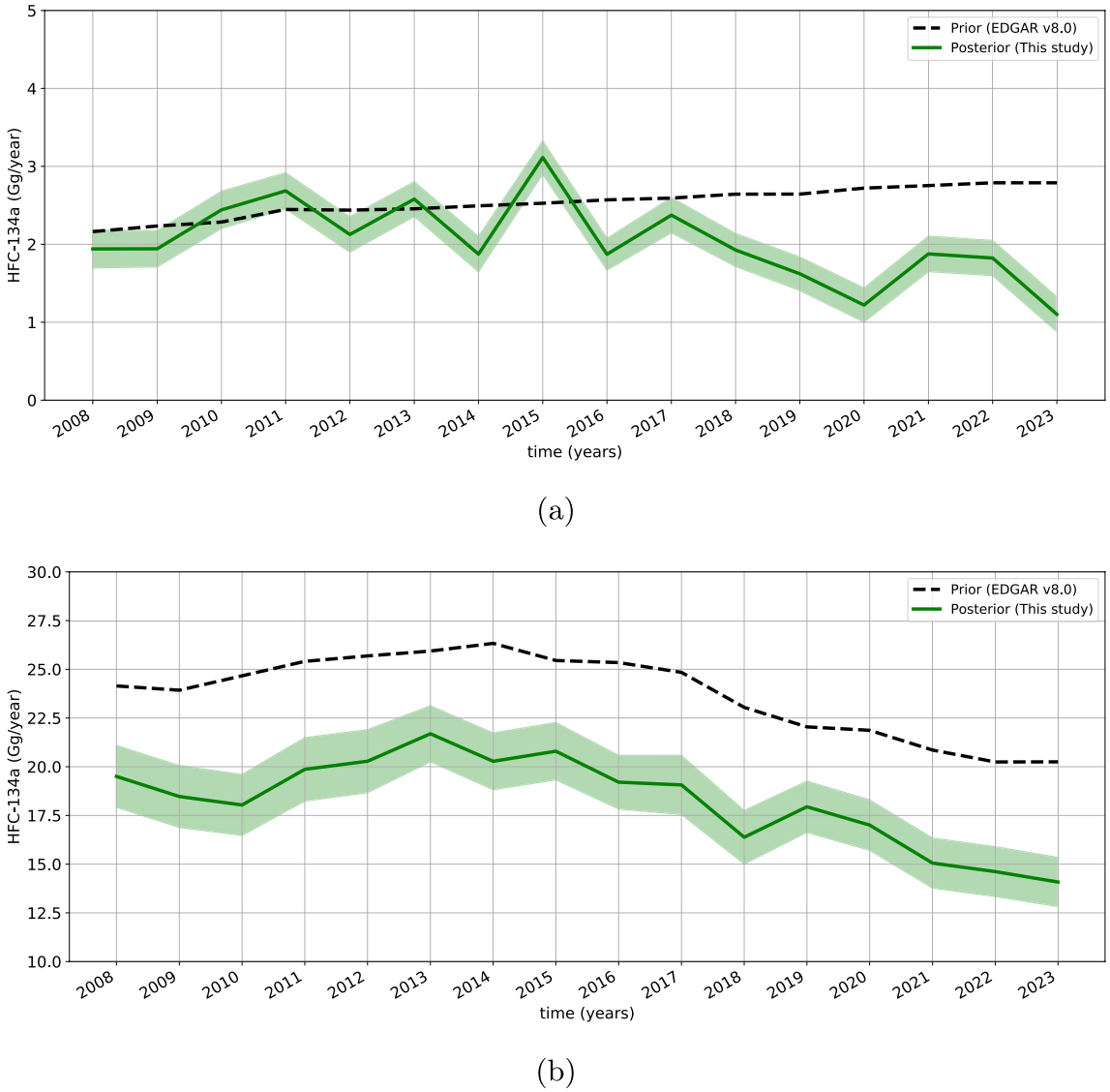


**Fig. 6** Comparisons between prior emissions estimates of HFC-134a according to EDGAR v8.0 (black dotted line) and yearly inversion estimates (green line) for **a** Italy, and **b** the European countries within the modelling domain, namely Austria, Belgium, Croatia, Czech Republic, Denmark, Finland, France, Germany, Hungary, Republic of Ireland, Italy, Luxembourg, the Netherlands, Norway, Poland, Portugal, Slovakia, Slovenia, Spain, Sweden, Switzerland, and the United Kingdom. Light green shadings show estimated uncertainty

inventories have undergone a continuous revision process incorporating new data, engaging additional stakeholders, and involving trade associations. This iterative process ensures that the inventories are progressively refined and updated to reflect the most accurate and comprehensive emission estimates. Such changes are highlighted in Fig. 7, where HFC-134a emission estimates from Italian NEIs for the main emission sector, i.e. refrigeration and air conditioning, for the study period are reported (plots for other sectors can be found in the Supplement (Figures S6 and S7)). 2012–2024 Italian NEIs can be clubbed into four groups with similar values, with the highest values given in the 2023 NEI, followed by the 2024 one, then those released in 2012, 2013, 2018–2022, and finally, 2014–2017.

In Fig. 8, we compared our inversion estimates with the values representative for each NEI group, EDGAR v8.0, and the top-down emission estimates from the study by [9]. The inversion results are in good agreement with both the NEI 2017 and 2022 and EDGAR v8.0 estimates until 2015. Emissions in [9] are slightly higher than our results. Estimates derived from inversion suggest that emissions began to decrease, albeit with some inter-annual fluctuations, after 2015, which better aligns with

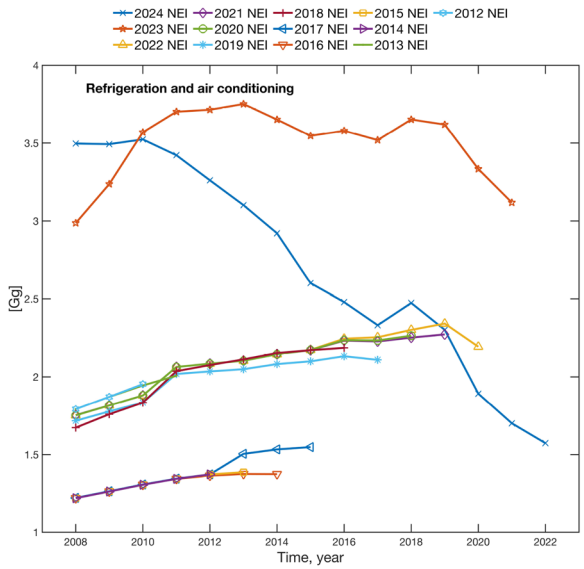


**Fig. 7** Comparison between the 2012–2024 Italian national emission inventories (NEIs) of HFC-134a emissions related to refrigeration and air conditioning. Own elaboration based on data from https://unfccc.int/ghg-inventories-annex-i-parties/2024

the trend and values obtained through the bottom-up approach in 2024.

To understand the differences between bottom-up and top-down estimates, we compared activity data, emission factors, and annual emissions reported in the last three NEIs (2022, 2023, and 2024) (Fig. 9) for specific parameters related to the highest contributing sector, i.e. mobile air conditioning (MAC). In NEI 2022, information on the product remaining at decommissioning, and thus disposal emissions, was missing. NEI 2023 provided estimates of the product remaining at disposal but reported no recovery, leading to high disposal emissions. In contrast, NEI 2024 provide emissions from disposal and recovery based on the amount of HFC-134a in products before decommissioning. The NEI 2024 revised the estimations of the consumption of HFC-134a in the MAC sector by refining the distribution of (i) consumption of HFC-134a among the various sub-sectors of use, and (ii) total consumption at first charge and at service. Consequently, NEI 2024 reports up to 81% lower average annual stock and 54% lower remaining product at decommissioning compared to NEI 2023, leading to a reduction of up to 69% in total MAC emissions for 2021. Additionally, NEI 2024 reports an average of 51% lower total MAC emissions for the period between 2008 and 2021. It is evident that differences among the latest NEIs, significantly impact emission estimates from the refrigeration and air conditioning sector and thus total HFC-134a emissions.

For the commercial refrigeration sector, the Italian national inventory report 2024 [25] also takes into account the technological advancements in equipment manufacturing and related leakage rates, as informed by the industrial associations. Specifically, the product life leakage rate decreased from 12.0% (2008–2014) to 10.0% (2015–2022) [25], lowering emissions from commercial refrigeration, which is the second-largest contributing sub-sector (Figure S8).

### Seasonal trends

For F-gases, the bottom-up emission inventories generally use constant emission factors throughout the year. Based on a literature review about the leakage of HFC refrigerants in refrigeration, air-conditioning, and heat

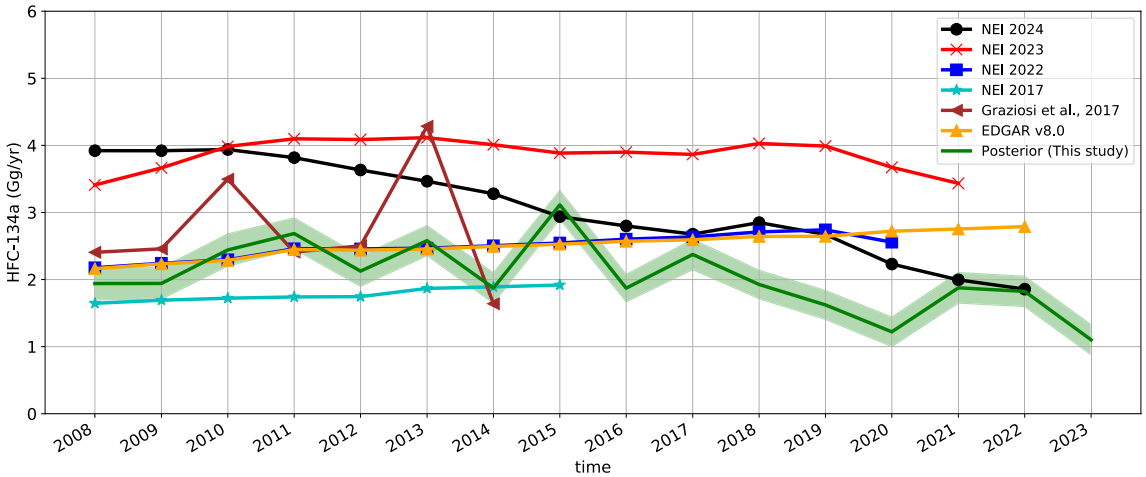


**Fig. 8** Comparison of emission estimates from Italy's National Emission Inventory (NEI) for 2017, 2022, 2023, and 2024, EDGAR v8.0, and the top-down estimates from this study

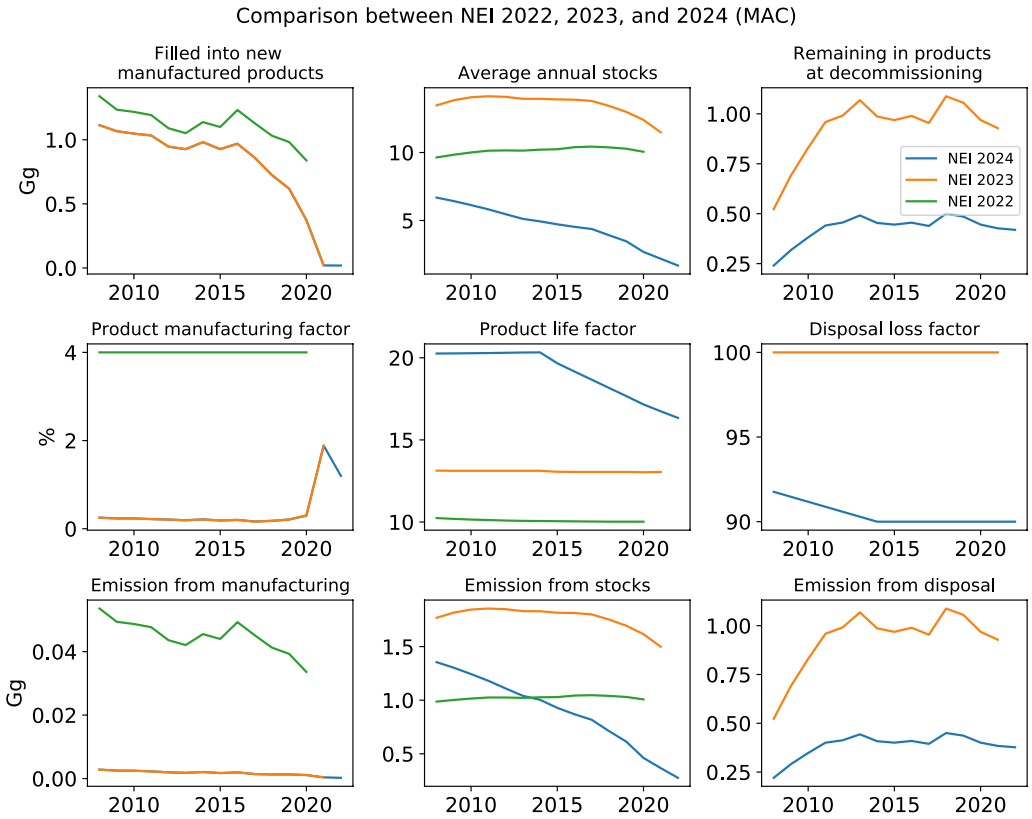


**Fig. 9** Comparisons between the NEI estimates of 2022, 2023, and 2024 for mobile air conditioning, showing activity data (row 1), emission factors (row 2), and annual emissions (row 3) for manufacturing (column 1), stocks (column 2), and disposal (column 3). Own elaboration based on data from https://unfccc.int/ghg-inventories-annex-i-parties/2024

pump systems, [22] concluded that the micro-sized leakages are the most common types of refrigerant leakages mainly due to mechanical wear and vibrations, which are more likely to occur during periods of higher usage of air-conditioning systems, namely in the summer months. The detrended monthly means of the observed mixing ratios are also statistically different (higher in summer months) based on a one-way unbalanced ANOVA analysis of variance (Figure S9). To investigate the seasonality in the Italian HFC-134a emissions and to support the bottom-up inventory compilation in considering such variations we performed monthly inversions. Figure 10 depicts detrended monthly inversion emission estimates for 2008–2023. Seasonal variation in HFC-134a emissions peaks during summer, coinciding with increased air conditioning use, with emissions and measurement signals particularly elevated in June and July. Our results show that, over the study period, in Italy, monthly mean emission estimates in summer (JJA) are 19.8% higher than in winter (DJF).

Hu et al. [12] have also reported a similar increase of 20–50% in HFC-134a emissions during summer compared to winter in the United States. [38] suggested that

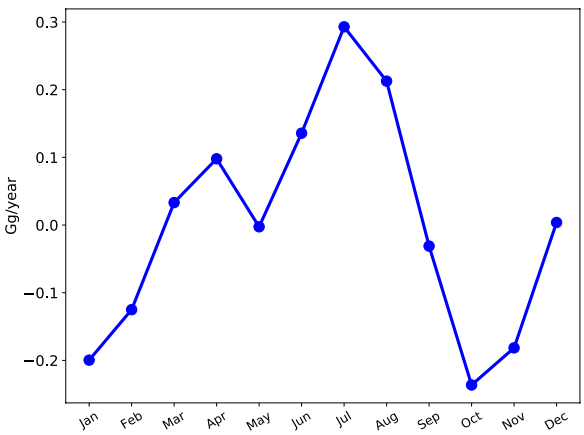


**Fig. 10** Monthly mean a posteriori emissions of HFC-134a for Italy from 2008 to 2023, detrended to remove long-term trend

higher ambient temperature and rate of use of mobile air-conditioning systems were drivers for up to three times higher HFC-134a emissions in summer compared to winter time. Previous studies have also reported seasonality of HFC-134a atmospheric abundance [26] and emissions

[12, 38]. In Switzerland, [26] recorded a seasonal variation in xHFC-134a ground-based Fourier transform infrared observations with a peak in August–September and a 4.5% peak-to-peak amplitude.

## Conclusion

This study presents a long-term estimation of HFC-134a emissions across Europe, with a particular focus on Italy from 2008 to 2023. The inversion estimates for Italy, showed the highest emissions in 2015 at $3.11 \pm 0.21$ Gg, which decreased to the lowest of $1.10 \pm 0.22$ Gg by 2023, indicating a downward trend. Over the period 2008–2023, Italian monthly mean emissions were 19.8% higher in summer compared to winter, pointing to a distinct seasonal pattern. The Po Valley, Italy's most polluted region, is a significant contributor to the country's total HFC-134a emissions. In 2020, the impact of mobility restrictions and lockdowns due to COVID-19 resulted in a reduction of MAC emissions, which is also reflected in our inversion-based estimates. The comparison of various Italian NEIs underscores the importance of annual updates and refinements in activity data and compilation processes. Our estimates, when compared with NEI 2024, significantly narrow the gap between top-down and bottom-up inventories for Italy.

In conclusion, this analysis shows that there is a decreasing trend in HFC-134a emissions for both Italy and the EU, underscoring the effectiveness of the EU F-gas regulations. We also provide a comprehensive comparison with bottom-up Italian NEIs to help reduce the gap between the two methods. This study highlights the need for further investigation to improve the accuracy of activity data and emission factors in bottom-up inventories. Additionally, our findings highlight the effectiveness of the inversion methodology in capturing emission changes related to seasonality and disruptive events like COVID-19.

## Supplementary Information

The online version contains supplementary material available at https://doi.org/10.1186/s12302-025-01081-1.

Supplementary Material 1.

**Acknowledgements**
We acknowledge the CINECA award under the ISCRA initiative for the availability of high-performance computing resources and support. We thank ECMWF for providing invaluable datasets to the research community. We are grateful to the Advance Global Atmospheric Gases Experiment (AGAGE) scientists at Scripps Institution of Oceanography (SIO, La Jolla, CA, USA) for maintaining and distributing the calibration scale. Finally, we would like to thank Steve Montzka (NOAA GML, Boulder, CO, USA) and Alistair Manning (UK Met Office, Exeter, UK) for useful discussions.

**Author contributions**
S.A., J.A., E.M., and M.M. conceptualised this work. S.A., J.A., and E.M. assessed methodology, formal analysis, and visualisation. S.A. wrote the original draft and S.A., E.M., B.G., F.M., S.OD., K.S., D.Y., R.C., U.G., M.M., and J.A. reviewed and edited the manuscript. U.G. and M.M. supervised and acquired funding for this research. B.G., F.M., S.D., K.S., D.Y., M.V., and J.A. performed data curation. S.A., R.C., and S.F. handled the software.

**Funding**
During this research work, Saurabh Annadate was supported by the Italian national inter-university PhD course in Sustainable Development and Climate Change (link:www.phd-sdc.it). Enrico Mancinelli's grant and measurement activities at Monte Cimone Station are funded under the Horizon Europe Project PARIS (Process Attribution of Regional Emissions, Project number 101081430). Serena Falasca gratefully acknowledges fellowship funding from MUR (Ministero dell'Università e della Ricerca) under PON "Ricerca e Innovazione" 2014–2020 (D.M. 1062/2021). The instrumentation at Monte Cimone was funded by the Italian component of ACTRIS (Aerosol, Clouds and Trace Gases Research Infrastructure), under the Programma Operativo Nazionale Ricerca e Innovazione 2014–2020. Measurements at Tacolneston and Mace Head were funded by the UK Department for Energy Security and Net Zero under contracts GA0201, TRN 1028/06/2015, TRN 1537/06/2018 and TRN 5488/11/2021. Mace Head measurements were also partially funded under NASA's Upper Atmosphere Research programme through grants NAG5-12669, NNX07AE89G, NNX11AF17G, and NNX16AC98G.

**Data availability**
Continuous atmospheric halocarbon measurement data for the AGAGE stations are available on the following website, http://agage.mit.edu/data/agage-data. FLEXPART footprints and FLEXINVERT+ model output files are available from the corresponding authors upon request. Input data used for running FLEXPART can be obtained from the ECMWF-ERA5 archive products, whose use is governed by the Creative Commons Attribution 4.0 International (CC BY 4.0), using the FLEX_exctract tool, URL: https://www.flexpart.eu/flex_extract/.

## Declarations

**Ethics approval and consent to participate**
Not applicable.

**Consent for publication**
Not applicable.

**Competing interests**
The authors declare that they have no conflict of interest.

**Author details**
[1]Department of Pure and Applied Sciences, University of Urbino "Carlo Bo", 61029 Urbino, Italy. [2]University School for Advanced Studies IUSS Pavia, Pavia, Italy. [3]Institute of Atmospheric Sciences and Climate, National Research Council, Bologna, Italy. [4]Institute for Environmental Protection and Research (ISPRA), Rome, Italy. [5]School of Chemistry, University of Bristol, Bristol BS8 1TS, UK. [6]Laboratory for Air Pollution and Environmental Technology, Empa, Swiss Federal Laboratories for Materials Science and Technology, 8600 Dübendorf, Switzerland. [7]Institute of Atmospheric Sciences and Climate, National Research Council, Lecce, Italy. [8]Department of Physics, Sapienza University of Rome, 00185 Rome, Italy.

Received: 4 September 2024 Accepted: 20 February 2025
Published online: 11 March 2025

**References**

1. An X, Henne S, Yao B et al (2012) Estimating emissions of HCFC-22 and CFC-11 in China by atmospheric observations and inverse modeling. Sci China Chem 55(10):2233–2241. https://doi.org/10.1007/s11426-012-4624-8

2. ANAS (2024) Dati di traffico medio giornaliero annuale. https://www.stradeanas.it/it/le-strade/osservatorio-del-traffico/dati-traffico-medio-giornaliero-annuale
3. Annadate S, Falasca S, Cesari R et al (2024) A sensitivity study of a Bayesian inversion model used to estimate emissions of synthetic greenhouse gases at the European scale. Atmosphere 15(1):51. https://doi.org/10.3390/atmos15010051
4. Brunner D, Arnold T, Henne S et al (2017) Comparison of four inverse modelling systems applied to the estimation of HFC-125, HFC-134a, and $SF_6$ emissions over Europe. Atmos Chem Phys 17(17):10651–10674. https://doi.org/10.5194/acp-17-10651-2017
5. EDGARv8.0 (2023) EDGAR—the Emissions Database for Global Atmospheric Research. Accessed 26 Mar 2024). https://edgar.jrc.ec.europa.eu/dataset_ghg80
6. EEA (2023) Fluorinated greenhouse gases 2023. data reported by companies on the production, import, export and destruction of fluorinated greenhouse gases in the european union, 2007–2022. eea report no 04/2023. luxembourg: Publications office of the European union
7. EUROSTAT (2024) Road motor vehicle traffic performance by traffic and registration location and type of vehicle. https://ec.europa.eu/eurostat/databrowser/view/road_tf_vehmov/default/table?lang=en
8. Giostra U, Furlani F, Arduini J et al (2011) The determination of a "regional" atmospheric background mixing ratio for anthropogenic greenhouse gases: a comparison of two independent methods. Atmos Environ 45(39):7396–7405
9. Graziosi F, Arduini J, Furlani F et al (2017) European emissions of the powerful greenhouse gases hydrofluorocarbons inferred from atmospheric measurements and their comparison with annual national reports to UNFCCC. Atmos Environ 158:85–97. https://doi.org/10.1016/j.atmosenv.2017.03.029
10. Harrison JJ, Chipperfield MP, Boone CD et al (2021) Fifteen years of HFC-134a satellite observations: comparisons With SLIMCAT calculations. J Geophys Res Atmos 126(8):e2020JD033208. https://doi.org/10.1029/2020JD033208
11. Henne S, Brunner D, Oney B et al (2016) Validation of the Swiss methane emission inventory by atmospheric observations and inverse modelling. Atmos Chem Phys 16(6):3683–3710. https://doi.org/10.5194/acp-16-3683-2016
12. Hu L, Montzka SA, Miller JB et al (2015) U.S. emissions of HFC-134a derived for 2008–2012 from an extensive flask-air sampling network. J Geophys Res Atmos 120(2):801–825. https://doi.org/10.1002/2014JD022617
13. Intergovernmental Panel on Climate Change IPCC (2023) The Earth's Energy Budget, Climate Feedbacks and Climate Sensitivity, Cambridge University Press. pp 923–1054
14. IPCC (2006) 2006 IPCC guidelines for national greenhouse gas inventories. https://www.ipcc-nggip.iges.or.jp/public/2006gl/
15. IPCC (2019) 2019 Refinement to the 2006 IPCC Guidelines for National Greenhouse Gas Inventories— IPCC. https://www.ipcc.ch/site/assets/uploads/2019/12/19R_V0_01_Overview.pdf
16. ISFORT (2023) 20° rapporto sulla mobilità degli italiani. https://www.isfort.it/wp-content/uploads/2023/12/RapportoMobilita2023_Def.pdf
17. ISPRA (2020) Le emissioni nazionali di gas serra settore traporti - 2020. https://emissioni.sina.isprambiente.it/wp-content/uploads/2022/12/Emissioni-Trasporti-Anno-2020-_def.pdf
18. Joint Research Centre (European Commission), Houweling S, Chevalier F et al (2018) Atmospheric monitoring and inverse modelling for verification of greenhouse gas inventories. Publications Office of the European Union. https://doi.org/10.2760/759928
19. Joint Research Centre (European Commission), Olivier JGJ, Guizzardi D, et al (2021) GHG emissions of all world: 2021 report. Publications Office of the European Union, https://data.europa.eu/doi/10.2760/173513
20. Katharopoulos I, Rust D, Vollmer MK et al (2023) Impact of transport model resolution and a priori assumptions on inverse modeling of Swiss F-gas emissions. Atmos Chem Phys 23(22):14159–14186. https://doi.org/10.5194/acp-23-14159-2023
21. Kim S, Kim EK (2015) Regular emission characteristics of hfc-134a from mobile air conditioners. J Ind Eng Chem 21:489–493
22. Li Y, Yang J, Wu X et al (2023) Leakage, diffusion and distribution characteristics of refrigerant in a limited space: a comprehensive review. Therm Sci Eng Progress 40:101731. https://doi.org/10.1016/j.tsep.2023.101731
23. Lunt MF, Rigby M, Ganesan AL et al (2015) Reconciling reported and unreported HFC emissions with atmospheric observations. Proc Nat Acad Sci 112(19):5927–5931. https://doi.org/10.1073/pnas.1420247112
24. Manning AJ, Redington AL, Say D et al (2021) Evidence of a recent decline in UK emissions of hydrofluorocarbons determined by the InTEM inverse model and atmospheric measurements. Atmos Chem Phys 21(16):12739–12755. https://doi.org/10.5194/acp-21-12739-2021
25. NIR (2024) Italian greenhouse gas inventory 1990-2022. national inventory report 2024. https://www.isprambiente.gov.it/files2024/pubblicazioni/rapporti/nir-2024-r-398-24.pdf
26. Pardo Cantos I, Mahieu E, Chipperfield MP et al (2024) First HFC-134a retrievals from ground-based FTIR solar absorption spectra, comparison with TOMCAT model simulations, in-situ AGAGE observations, and ACE-FTS satellite data for the Jungfraujoch station. J Quant Spectrosc Radiat Transfer 318:108938. https://doi.org/10.1016/j.jqsrt.2024.108938
27. Pisso I, Sollum E, Grythe H et al (2019) The Lagrangian particle dispersion model FLEXPART version 10.4. Geosci Model Dev 12(12):4955–4997. https://doi.org/10.5194/gmd-12-4955-2019
28. Prinn RG, Weiss RF, Arduini J et al (2018) History of chemically and radiatively important atmospheric gases from the advanced global atmospheric gases experiment (agage). Earth Syst Sci Data 10(2):985–1018. https://doi.org/10.5194/essd-10-985-2018
29. Ruckstuhl AF, Henne S, Reimann S et al (2012) Robust extraction of baseline signal of atmospheric trace species using local regression. Atmos Measure Tech 5(11):2613–2624. https://doi.org/10.5194/amt-5-2613-2012
30. Rust D, Katharopoulos I, Vollmer MK et al (2022) Swiss halocarbon emissions for 2019 to 2020 assessed from regional atmospheric observations. Atmos Chem Phys 22(4):2447–2466. https://doi.org/10.5194/acp-22-2447-2022
31. Say D, Manning AJ, O'Doherty S et al (2016) Re-evaluation of the UK's HFC-134a emissions inventory based on atmospheric observations. Environ Sci Technol 50(20):11129–11136. https://doi.org/10.1021/acs.est.6b03630
32. Schoenenberger F, Henne S, Hill M et al (2018) Abundance and sources of atmospheric halocarbons in the Eastern Mediterranean. Atmos Chem Phys 18(6):4069–4092. https://doi.org/10.5194/acp-18-4069-2018
33. Stohl A, Seibert P, Arduini J et al (2009) An analytical inversion method for determining regional and global emissions of greenhouse gases: sensitivity studies and application to halocarbons. Atmos Chem Phys 9(5):1597–1620
34. Thompson RL, Stohl A (2014) FLEXINVERT: an atmospheric Bayesian inversion framework for determining surface fluxes of trace species using an optimized grid. Geosci Model Dev 7(5):2223–2242. https://doi.org/10.5194/gmd-7-2223-2014
35. United Nations (2016) Kigali amendment, united Nations Treaty Collection. https://treaties.un.org/Pages/ViewDetails.aspx?src=IND&mtdsg_no=XXVII-2-a &chapter=27 &clang=_en
36. Vojta M, Plach A, Thompson RL et al (2022) A comprehensive evaluation of the use of Lagrangian particle dispersion models for inverse modeling of greenhouse gas emissions. Geosci Model Dev 15(22):8295–8323. https://doi.org/10.5194/gmd-15-8295-2022
37. World Meteorological Organization WMO (2022) Scientific Assessment of Ozone Depletion: 2022, GAW Report No. 278, 509 pp.; WMO: Geneva
38. Xiang B, Patra PK, Montzka SA et al (2014) Global emissions of refrigerants HCFC-22 and HFC-134a: unforeseen seasonal contributions. Proc Nat Acad Sci 111(49):17379–17384. https://doi.org/10.1073/pnas.1417372111
39. Zhang Y, Yang W, Huang Z et al (2017) Leakage rates of refrigerants cfc-12, hcfc-22, and hfc-134a from operating mobile air conditioning systems in guangzhou, china: tests inside a busy urban tunnel under hot and humid weather conditions. Environ Sci Technol Lett 4(11):481–486


## Publisher's Note